J Mater Sci (2007) 42:8150–8157
DOI 10.1007/s10853-007-1703-x

Mechanical characterization of glass/polyimide microjoints fabricated using cw fiber and diode lasers

Ahsan Mian · Golam Newaz · Tonfiz Mahmood · Greg Auner

Received: 5 June 2006 / Accepted: 16 March 2007 / Published online: 9 June 2007
© Springer Science+Business Media, LLC 2007

Abstract This paper discusses the laser-irradiated microjoints between glass and polyimide for applications in neural implants. To facilitate bonding between them, a thin titanium film with a thickness of approximately 0.2 μm was deposited on glass wafers using the physical vapor deposition (PVD) process. Two sets of samples were fabricated where the bonds were created using diode and fiber lasers. The samples were subjected to tension using a microtester for bond strength measurements. The failure strengths of the bonds generated using fiber laser are quite consistent, while a wide variation of failure strengths are observed for the bonds generated with diode laser. Few untested samples were sectioned and the microstructures near the bond areas were studied using an optical microscope. The images revealed the presence of a sharp crack in the glass substrate near the bond generated with the diode laser. However, no such crack was observed in the samples made using fiber laser. To investigate the reasons behind such discrepancy in bond quality further, uncoupled three-dimensional finite element analyses (FEA) were conducted only for the samples created using diode laser. First, the transient heat diffusion-based FEA was conducted by using the laser power intensity distribution as a time dependent heat source. This model calculates the temperature distribution within the substrates as a function of time. Next, the structural model predicts the amount of residual stresses developed in the joint system as it is cooled down to room temperature. The out-of-plane normal component of residual stresses was within the failure strength range of glass that may have caused fracture initiation in the substrate.

A. Mian (✉)
Department of Mechanical and Industrial Engineering,
Montana State University, 220 Roberts Hall,
Bozeman, MT, USA
e-mail: amian@me.montana.edu

G. Newaz · T. Mahmood
Department of Mechanical Engineering,
Wayne State University, Detroit, MI, USA

G. Auner
Department of Electrical and Computer Engineering,
Wayne State University, Detroit, MI, USA

Introduction

Novel biomedical products, implantable microsystems in particular such as devices that electrically stimulate and/or record neural activity [1–6], are designed with a high level of device integration and miniaturization that pose new challenges to their assembly and packaging. Such devices may include various biocompatible materials such as glass, ceramic and polymers that must be reliably joined in similar and dissimilar combinations. Conventional joining techniques such as the use of adhesives have several drawbacks such as they often lack long-term stability, shrink during curing, and sometimes do not meet biocompatibility requirements. High heat input during soldering or brazing may potentially damage the implant electronics that are being packaged. The common disadvantage of all of the conventional joining processes is that they do not perform well for localized bonding at the submillimeter scale. These limitations can be overcome by laser joining techniques that intrinsically provide excellent focusing to spot sizes in the micrometer range. In addition, the precise control of the laser power in the focal spot enables highly localized processing with minimum heat effect outside the joint region.

Recently, the chemical and physical nature of sub-millimeter joints between polyimide and bulk titanium fabricated using laser in ambient conditions has been studied. The results showed the presence of a very sharp interface of thickness about 10 nm. The XPS study of the interface revealed the creation of chemical bonds between titanium and oxygen, and titanium and carbon [7]. It is mentioned here that the source of such carbon and oxygen bonds with titanium is the carbonyl groups >C=O present in polyimide. Presence of TiO_2 particles and Ti–C bonds at such titanium/polyimide interfaces generated in clean, vacuum conditions is also evidenced in references [8, 9]. As the feasibility of joining polyimide to titanium using laser has been verified [7, 10–12], the next step was to identify the appropriate processing parameters that permits the creation of good hermetic joints between titanium coated borosilicate glass (TiBSG) and polyimide (PI). To accomplish this goal in part, the joints between PI and TiBSG processed using two types of lasers are characterized using tensile mechanical failure tests and optical microscopy. This study will provide an understanding of how the types of laser influence the quality of laser irradiated microjoints.

In this study, two sets of laser-bonded samples were processed. One set of the samples was prepared with a cw diode laser, while the other set was processed using a cw fiber laser. Both types of samples were mechanically tested using a tensile microtester. The bond failure load obtained from such testing represents the bond quality. Since the laser joining process is characterized by the highly collimated and concentrated beam energy, residual stresses are likely to be introduced into the laser-processed microjoints as a consequence of incompatible thermal strains caused by heating and cooling cycles during the manufacturing process. These stresses are even higher in case of joining dissimilar materials due to the mismatches in their coefficients of thermal expansion (CTE). To understand the stress distribution within the bond regions, three-dimensional uncoupled finite element analysis (FEA) was conducted only for the samples created with diode lasers.

Materials and sample preparation

In this paper, we have investigated laser-irradiated joints between borosilicate glass and polyimide. To facilitate bonding between them, a thin titanium film with a thickness of approximately 0.2 μm was deposited on glass wafers using the physical vapor deposition (PVD) process. Titanium film was selected as a coupling agent as the existence of chemical bonds at the laser-processed titanium/polyimide microjoint interfaces has already been identified [7]. In addition, titanium is an excellent biocompatible material. The transmission laser microjoining process that has been demonstrated in details in reference [12] was utilized in this case to create bonds between TiBSG and PI. In this process, the joining material combination includes one absorbent (in this case, titanium) and one transparent (in this case, polyimide) part at the laser wavelength. The laser energy penetrates polyimide and is absorbed by titanium, so that the heat is induced directly at the interface. The temperature at the interface exceeds the melting point of polyimide and is sufficient to create chemical bonds between titanium and polyimide. The transmission laser microjoining process is shown schematically in Fig. 1.

Two sets of laser-bonded samples were processed. One set of the samples was prepared with a 0.8 μm cw diode laser using a laser power of 3.0 W. The other set of samples was processed using a 1.1 μm Yb-doped cw fiber laser (1.0 W). It is mentioned here that the spot diameters for the diode and fiber lasers were 800 μm and 200 μm, respectively. For both sets of the samples, the laser head was scanned at a speed of 100 mm/min along the width of the sample to generate a 6.5 mm long bond. Schematic of the samples is shown in Fig. 2. It is mentioned here that the

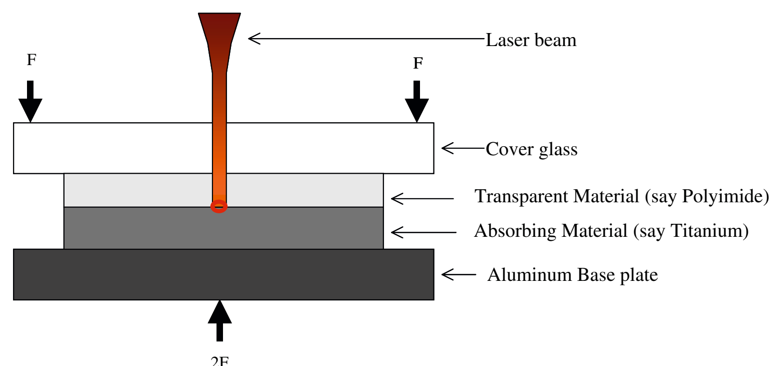

Fig. 1 Transmission joining of two materials using a laser beam

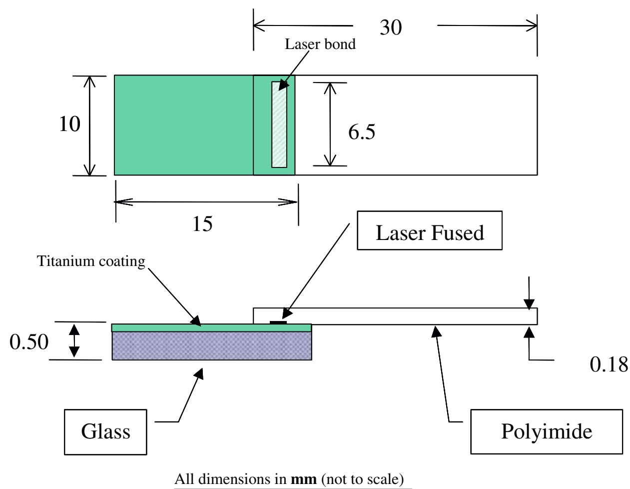

Fig. 2 Schematic of a tensile sample

diode and fiber lasers had super-Gaussian and Gaussian type intensity distributions, respectively.

Experimental

Experimental methods

The samples created using both the laser systems were tested for bond strengths using a microtester. The testing machine used in this case is called a 6-axis sub-micron tester [10–14], which is a general-purpose micromechanical/thermal testing instrument. The machine is fully controlled by a computer, and can be operated both in displacement and load controls along six degrees of freedom, i.e., three orthogonal translations and three rotations. The displacement resolution of each closed-loop, DC-motor-drive stage is maintained at 0.1 mm in translations and 0.001 degree in rotations. A capacitance gage installed in the equipment measures the actual displacement of a test sample. The samples were loaded in the fixture of the testing machine and were subjected to uniaxial tension by turning on the motor that moves in the sample's length direction. The software that controls the machine also acquires load cell and capacitance gage information (load-displacement data).

Several untested samples were also sectioned at the bond region and were analyzed using an optical microscope. The samples were sectioned carefully using a diamond cutter and were molded in epoxy. A diamond polisher was used to polish the epoxy molded sectioned samples.

Experimental results

All of the fabricated samples were loaded in tension until failure. The failure loads obtained for all samples were divided by the corresponding bond lengths to calculate the failure load per unit bond length. The bond lengths were measured using an optical microscope prior to testing the samples. Test results for both types of samples are presented in Table 1. The average failure strength of the six samples processed using diode laser was observed to be 6.19 N/mm with standard deviation of 2.7 N/mm. On the other hand, the samples created using fiber laser had higher bond strength (7.34 N/mm) with a relatively small standard deviation of 0.46 N/mm. To understand the reason behind these wide variations in bond strengths for the diode laser-processed samples, several samples were sectioned and viewed under an optical microscope.

Table 1 Bond strength of the samples processed with diode and fiber lasers

Laser used	Average bond strength (N/mm)	Standard deviation (N/mm)	Number of samples tested
Diode laser	6.19	2.7	6
Fiber laser	7.34	0.46	6

Figure 3 shows representative images of the sectioned samples. A large crack was observed in the glass substrate for the diode laser-processed sample, which is evidenced in Fig. 3a. However, no such crack was seen in the cross-section of the sample created with fiber laser (Fig. 3b). It is thus reasonable to believe that some of the samples that were tested for bond strength had cracks and hence had very low failure loads. The use of diode laser may have introduced higher residual stresses in the substrate during joint fabrication than the fiber laser did. This may be due to the fact that the diode laser has very different power distribution (which is super-Gaussian) than the fiber laser (Gaussian).

Finite element methods

The FEA technique was utilized next to verify the amount of residual stresses developed for the case of diode laser which may have caused substrate fracture. The moving cw diode laser beam with super-Gaussian intensity distribution strikes the titanium surface at the titanium/polyimide interface. The problem of thermal mechanical stress analysis was solved in a decoupled manner using finite element software ABAQUS [15]. First the heat flow problem was solved by considering a moving heat source. The time dependent 3-D temperature profile over the sample was then used to solve for the residual stress as the model was to be cooled down to room temperature. Due to the presence of loading and material symmetries, only half model was considered (Fig. 4). Here only the overlap portion was considered as the heat flow to the

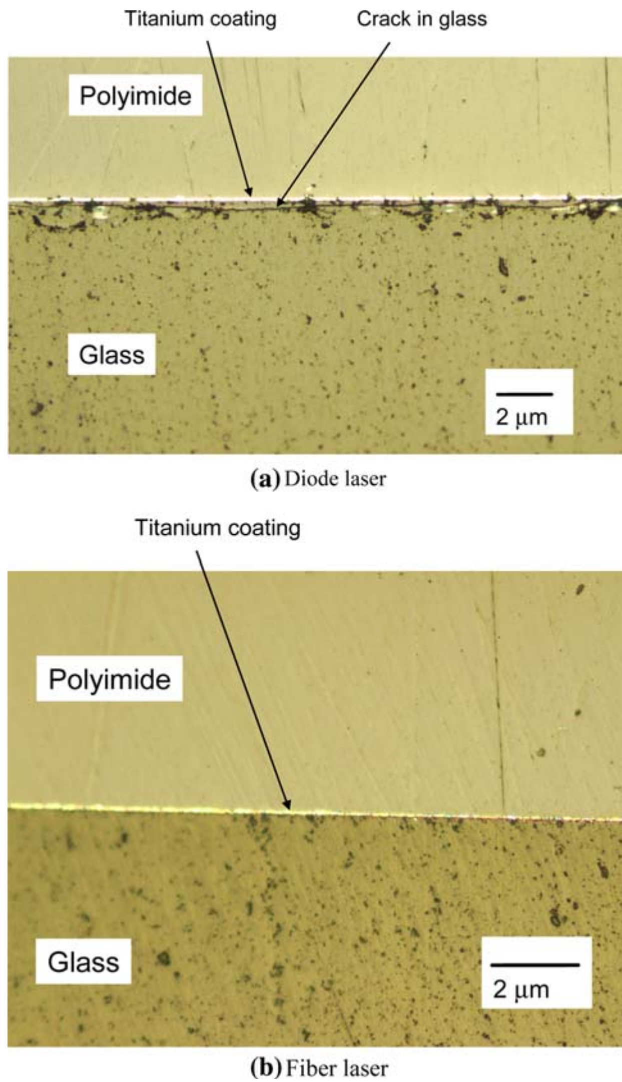

Fig. 3 Optical micrographs of cross-sections of the samples processed with diode and fiber lasers

region away from the bond area can be considered negligible, and hence those areas are not considered in the calculation. The thickness and width of the model in Fig. 4 represent true dimensions of the sample that was used for experiments that is given in Fig. 2. The solution steps are outlined next.

Thermal analysis

Model development

A solid body heat conduction model was developed to calculate the temperature distribution in and around the laser-irradiated areas. All three materials, such as titanium, glass, and polyimide, were modeled using eight-noded (type DC3D8) and six-noded (type DC3D6) diffusive heat transfer elements with one degree of freedom (temperature) at each node. Figure 5 shows the developed FEA model that also shows the zoomed-in mesh view near the interface. The interface between the joining materials was modeled using thermal interface elements. In this case, the mating surfaces at the interface were modeled by using two separate sets of nodes. The two sets of nodes belong to the two different element sets corresponding to the two materials at the interface. The heat flow across the interface was considered via both conduction and radiation. The moving circular laser was modeled as a distributed heat flux on the material surface on which the laser is being focused (which is titanium in this case). This heat flux was calculated as follows from the total power and power distribution. For super Gaussian distribution

$$q = \frac{Q}{\pi \bar{r}^2} \tag{1}$$

where $\bar{r}$is the characteristic radius (defined as the radius at which the intensity of the laser beam falls to 5% of the maximum intensity) and Q is the power transferred into the material. In our calculation, Q and $\bar{r}$were considered to be 3.0 W and 400 μm (which is nothing but the diode laser beam radius), respectively.

The material properties required for the heat flow analysis are thermal conductivity, specific heat, density and latent heat for all of the materials. The material properties were obtained from reference [16] and are given in Table 2. For simplicity, phase change of polyimide during this laser processing was not considered. The initial condition for the entire solution domain was room temperature. On all of the surfaces, both natural convection and radiation were considered as a boundary condition. Due to

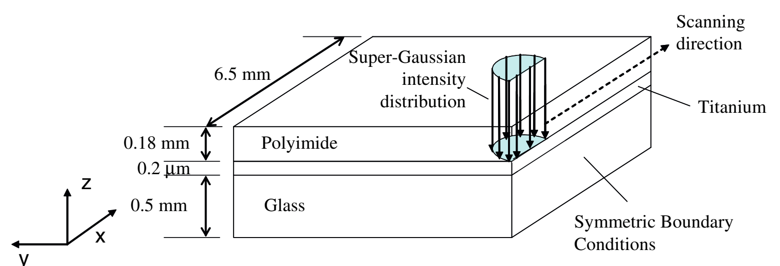

Fig. 4 Half model near the bond region with symmetric boundary conditions (diode laser)

Table 2 Thermal and mechanical properties of the materials used in the FEA models

Material	Density ρ (kg/m^3)	Modulus of elasticity, E (GPa)	Poisson's ratio, ν	Coefficient of thermal expansion, α (μm/m- °C)	Specific heat capacity, C_p (J/kg-°C)	Thermal conductivity, k (W/m-K)
Polyimide	1,380	1.35	0.41	60	1,130	0.25
Titanium	4,400	116.0	0.34	8.9	530	17.0
Borosilicate glass	2,400	62.0	0.2	4.0	830	1.1

symmetric nature of the system, only one half of the materials are considered. The plane of symmetry in this case is the plane through which the beam center moves. An insulated boundary condition was imposed on the symmetric surface. The moving heat source was modeled by reassigning the location of the distributed heat flux calculated using Eq. (1) at different time steps. The time was calculated based on the scanning velocity and heat source location. The transient heat transfer model was then run and nodal temperature was documented as a function of time for use in the subsequent steps.

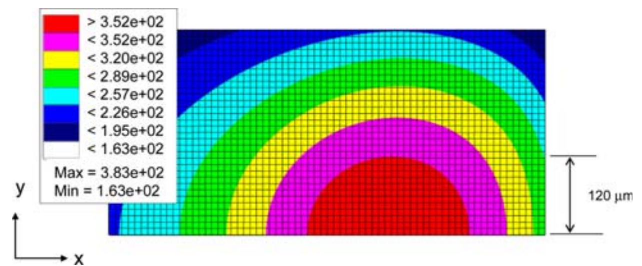

Fig. 6 Temperature distribution in polyimide at the polyimide/titanium interface (diode laser). The size of the heat-affected zone that has temperature above 350 °C is 120 μm

Results from thermal model

At the end of transient analysis, nodal temperatures were recorded as a function of time. The temperature field was observed to change with time as the heat source was moving along the width of the sample. Figure 6 shows the instantaneous temperature distribution in polyimide at the titanium/polyimide interface when the laser head (or moving heat source) traveled for 1.0 s at the scanning speed of 100 mm/min. It is clear from the contour plot that the size of the heat-affected zone (HAZ) that has temperature above 350 °C is 120 μm. It is mentioned here that the melting point of polyimide is 350 °C. So, it is reasonable to consider that the HAZ in polyimide having temperature above its melting point will create bond. Thus, the size of the bond should be 240 μm (double of 120 μm as Fig. 6 represents a half model) which is similar to the experimentally measured bond width as published in reference [10]. The residual stresses development in the joint is calculated next using a separate FEA model as the system is now cooled down from the processing temperature (the nodal temperatures recorded in this step) to room temperature.

Structural analysis

Model development

In this case, the finite element model employed the same discretized model as used in the thermal analysis except that now the model will be utilized for stress analysis. In addition, half the bond width between titanium and polyimide was considered as 120 μm (Fig. 7) as was determined from the thermal model. The laser irradiated 120 μm bond between titanium and polyimide as well as the titanium-

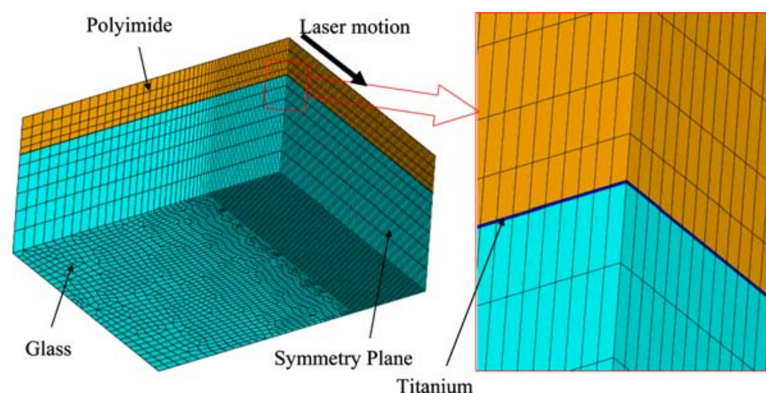

Fig. 5 FEA model along with a zoomed-in mesh view (same mesh used for both the thermal and structural model)

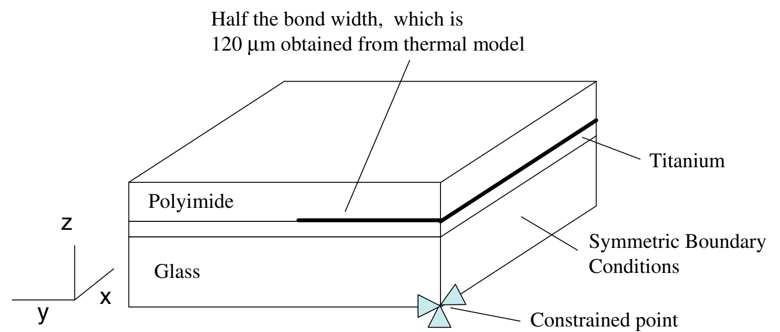

Fig. 7 Half model near the bond region for structural analysis. Half-bond width is 120 μm, which is obtained from the thermal model

glass interface were considered to be strong. These strong bimaterial interfaces were modeled by using a common set of nodes at the glass-titanium and titanium-polyimide interfaces. The common interfacial nodes are shared by elements corresponding to both titanium and polyimide for the titanium-polyimide bond interface. Similarly, the common set of nodes at the glass-titanium interface is shared by the elements corresponding to the glass and titanium substrates. Symmetry boundary conditions were applied at the symmetry surface such that the translations have no component normal to the plane of symmetry. In other words, at the symmetry face displacement v is constrained while displacements u and w are free so that Poisson effects can take place in the x and z directions in that face. One corner of the model was fully constrained so that all other nodes can move with respect to this fixed node. The applied boundary conditions are shown schematically in Fig. 7.

Two material models were used in the study: a simple linear elastic, and a linear elastic–plastic models. The substrate glass was modeled as linear elastic, while polyimide and titanium was modeled as elastic–plastic. The linear-elastic model is an ABAQUS standard material model, which requires two properties: the modulus of elasticity and Poisson's ratio (Table 2). The elastic–plastic model used for polyimide and titanium utilizes the classic von Mises yield criterion, which is also available in ABAQUS. The model requires modulus of elasticity, Poisson's ratio (Table 2), and stress–strain data in the plastic region. The stress–strain responses of polyimide and titanium are given in Table 3 that was used to input the plastic portion of the curve. Due to the large deformation of polyimide, geometric nonlinearily was included in the calculation so that the stiffness matrix can updated at each incremental applied load based on the deformation of the joining materials.

Table 3 Stress–strain data for polyimide and titanium used in FEA

	Polyimide			Titanium		
Stress (MPa)	0	70.0	118	0	140.0	220.0
Strain (m/m)	0	0.023	1.1	0	0.0012	0.54

The joining assembly was cooled down from the process induced nodal temperature obtained in the thermal analysis step to room temperature, and the residual stress was calculated. The model was considered stress free at the solidification (or melting) temperature of polyimide, which is 350 °C. Thus, the nodes that had instantaneous temperature above 350 °C were considered to have the initial temperature as 350 °C.

Results from structural model

In this paper, the stresses developed only in the glass substrate are analyzed as the micrographs showed the presence of a crack only in glass. It was observed that the in-plane normal stresses (σ_x and σ_y) were all compressive which is expected. This is due to the fact that the CTE for glass is lower than both polyimide and titanium and that the joining system is cooled down from the stress free temperature (350 °C) to room temperature. The maximum in-plane normal stress was found to be 360 MPa and is well below the compressive strength of glass which is about 700 MPa (source: http://www.matweb.com). Thus, no failure is expected due to these compressive normal stresses and hence detailed description of in-plane normal stress distributions is not presented here.

Variations of out-of-plane normal (σ_z) and in-plane shear (τ_{xy}) stresses developed in glass at the glass-titanium interface along the bond width are shown in Figs. 8 and 9, respectively. The graphs also included these stress variations at different planes normal to the bond length direction. The locations of these planes are shown along with the stress plots. Due to geometric and material singularity, large variations of stresses are expected near the two sides (e.g., left and right) of the bond. It is evident from both Figs. 8 and 9 that the stress variation is steeper at the sides while a lower level stress is developed over the region near the longitudinal mid section. Maximum z-direction stress is found to be 61.0 MPa near the corner of the bond area (the maximum stress location is 80 μm from the edge and about

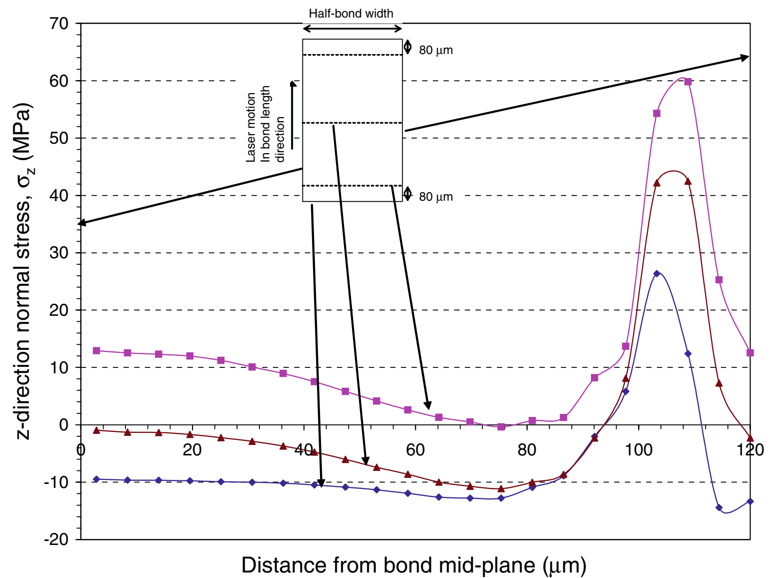

Fig. 8 Variation of out-of-plane normal stress at the glass-titanium interface in glass at various locations. The stress was developed as the joining system was cooled down from process temperature to room temperature

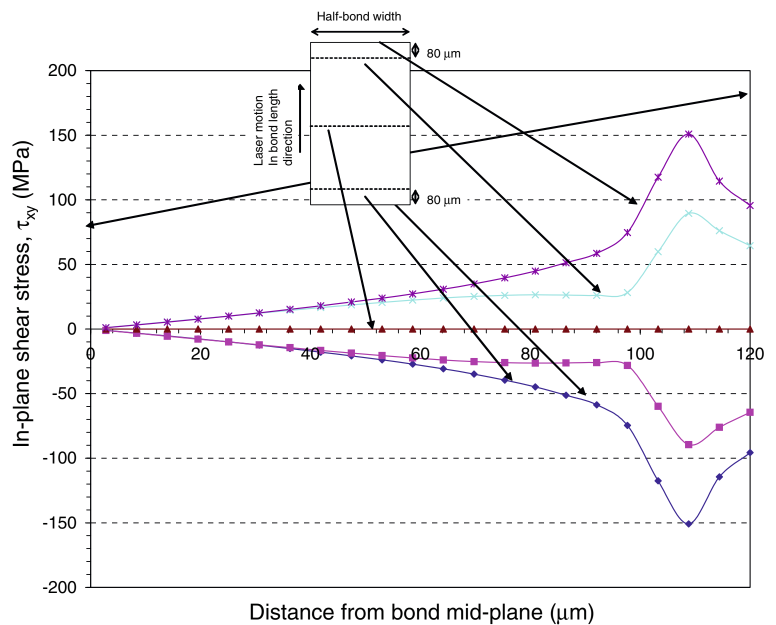

Fig. 9 Variation of in-plane shear stress at the glass-titanium interface in glass at various locations. The stress was developed as the joining system was cooled down from process temperature to room temperature

15 μm from the side of the bond) which is close to the average breaking strength of borosilicate glass of 70 MPa [17]. It is mentioned here that the lack of ductility of glass prevents the equalization of stresses at local irregularities or flaws and hence the tensile strength of glass *varies considerably* about a mean value. Thus, it is not surprising to see that some of the samples may have experienced failure initiation at a lower stress level of 61 MPa. The in-plane shear stress as shown in Fig. 9 is zero at the both transverse and longitudinal mid-planes and increases with the distance from the mid-planes. The peak shear stress is 151 MPa right on the edge however about 12 μm away from the side. This high in-plane shear stress along with other out-of-plane shear stress components (τ_{xz}, τ_{yz}) may cause crack propagation that was initiated due to high *z*-component normal stress. It is worth mentioning that the out-of-plane shear stress components are small compared to τ_{xy}, and hence are not presented in this paper.

Summary

In this study, the joints between titanium coated glass and polyimide created by cw fiber and diode lasers are mechanically characterized for their potential use in bio-encapsulation applications. It is observed that the fiber laser

created joints have higher bond strength (7.34 N/mm) than the diode laser created joints (6.19 N/mm). Optical microscopy of the joints fabricated using diode lasers revealed the presence of cracks in the glass substrate. To further investigate the factors responsible for such cracks, three-dimensional uncoupled finite element modeling was employed for the diode laser-processed samples. Two FEA models, namely thermal and mechanical, were developed. The thermal model was used to model the laser process that solves the transient heat diffusion equations. The structural model calculated the stresses developed in the joining materials as the system is being cooled from the laser process induced nodal temperature (obtained from the thermal model) to room temperature. Stress analysis showed the development of large residual stresses (e.g., σ_z = 61 MPa) in glass that is within the failure strength range. This residual stress component is the main source of substrate cracks as was observed in the diode laser-processed samples.

Acknowledgements The authors acknowledge the financial support from Michigan Economic Development Corporation (MEDC), and Michigan Life Sciences Corridor Grant GR-358 to perform this study.

References

1. Ludwig K, Uram J, Yang J, Martin D, Kipke D (2006) J Neural Eng 3:59
2. Subbaroyan J, Martin D, Kipke D (2005) J Neural Eng 2:103
3. Hung A, Zhou D, Greenberg R, Judy J (2002) Proceedings of the IEEE Micro Electro Mechanical Systems (MEMS), Las Vegas, NV, USA, January 2002, p 56
4. Techer JD, Bernard S, Bertrand Y, Cathebras G, Guiraud D (2004) IEEE International Workshop on Biomedical Circuits and Systems, Singapore, December 2004
5. White AR, Hawke SH (2003) J Neurochem 87:801
6. Deuschl G, Wenzelburger R, Kopper F, Volkmann J (2003) J Neurol Suppl 250:43
7. Georgiev DG, Baird RJ, Newaz G, Auner G, Herfurth H, Witte R (2004) Appl Surf Sci 236:71
8. Girardeaux C, Druet E, Demoncy P, Delamar M (1994) J Electron Spectrosc Relat Phenom 70:11
9. Ohuchi FS, Freilich SC (1986) J Vac Sci Technol A 4:1039
10. Mian A, Newaz G, Vendra L, Rahman N, Georgiev DG, Auner G, Witte R, Herfurth H (2005) J Mat Sci: Mater Med 16:229
11. Newaz G, Mian A, Sultana T, Mahmood T, Georgiev D, Witte R, Herfurth H, Auner G (2006) J Biomed Mat Res 79A:159
12. Mian A, Newaz G, Georgiev DG, Rahman N, Vendra L, Auner G, Witte R, Herfurth H (2007) J Mat Sci: Mater Med 18:417
13. Bauer I, Russek UA, Herfurth H, Witte R, Heinemann S, Newaz G, Mian A, Georgiev DG, Auner G (2004) Proceedings of SPIE—Photonics West LASE 2004: Lasers and Applications in Science and Engineering conference, 24–29 January 2004, San Jose, California 5339, 454
14. Lu M, Qian Z, Ren W, Liu S, Shangguan D (1999) Int J Solid Struct 36:65
15. ABAQUS User's Manual, Version 6.2, Hibbit, Karlsson and Sorensen, USA
16. http://www.matweb.com, as on 11 March 2007
17. http://www.pegasus-glass.com/pyrex.asp, as on 11 March 2007